Frequency shift in three-photon resonant four-wave mixing by internal atom-field interaction

Natalia R. de Melo* and Sandra S. Vianna†
Departamento de Física, Universidade Federal de Pernambuco, 50670-901 Recife, Pernambuco, Brazil
(Received 6 July 2015; published 11 November 2015)

We report on experimental results of four-wave mixing processes in rubidium vapor where coherence is induced on the three-photon resonant transition from $5s$ to $6p$ states via intermediate Rydberg levels. It is shown that the use of two beams in a noncollinear configuration, i.e., $\theta \neq 0$, and high atomic density unveil new features. First, the $\theta = 0$ (collinear configuration) odd-photon destructive interference between the incident and generated fields is strongly inhibited for $\theta \neq 0$. Second, most importantly, the observed cooperative frequency shift of the three-photon transition is strongly enhanced for small, but nonzero, values of θ due to the factor $(1 - \cos\theta)^{-1}$, which is not present if the generated radiation field is not considered self-consistently in the Maxwell-Bloch equations.

DOI: 10.1103/PhysRevA.92.053830 PACS number(s): 42.65.Ky, 32.80.Qk, 42.50.Gy

I. INTRODUCTION

Modifications of resonant absorption and emission spectral lines by dense atomic samples are of fundamental importance in the investigations of a variety of quantum and nonlinear phenomena. In fact, intriguing properties can be obtained when many atoms collectively interact via a common electromagnetic field, such as superradiance [1] and cooperative frequency Lamb shift [2,3]. Recently, the latter N-atom phenomenon was shown to play a prominent role in distinct experiments: evidence of connection to the superradiance of resonant ^{57}Fe nuclei [4], Rb vapor confined in a cell of tunable thickness [5], and a mesoscopic array of Sr^+ ions in a Paul trap [6]. Moreover, effects due to the competition between different excitation pathways [7,8] or quantum interference with the internally common radiation field [9,10] have also been explored, under resonant conditions, using nonlinear phenomena. In this scenario, nonlinear four-wave mixing (FWM) processes involving highly excited Rydberg atoms appear to be a promising laboratory to investigate the phenomena caused by N-atom interaction induced by the generated radiation field. We also remark that two-photon resonant FWM can be used to generate new frequencies with possible applications for quantum communication [11] and quantum information processing [12,13].

In this work, we apply FWM techniques to study the nonlinear response of a thermal rubidium sample in which coherence is induced on the three-photon resonant transition from $5s$ to $6p$ states via Rydberg levels and to investigate the associated cooperative frequency shift induced by the interaction between the atoms through the reabsorption of photons of the generated radiation field. The above-mentioned three-photon resonance has already been investigated in a collinear beam configuration, i.e., $\theta = 0$, and low atomic density [14]. Under these conditions, interference between different excitation pathways was studied for the case when two neighboring Rydberg levels play the role of near two-photon resonant intermediate levels. Recently [15], we also investigated this system in the high-atomic-density regime but maintaining the collinear beam configuration. In these conditions, a collision-induced broadening of the two-photon resonant lines was observed, as well as an odd-photon destructive interference involving the incident and generated fields [16].

The main focus of the present investigation is to show that the use of the noncollinear beam configuration, i.e., $\theta \neq 0$, and high atomic density unveil new features, in which case propagation effects such as absorption and phase matching are important. At the three-photon resonance, two main effects are observed: first, the $\theta = 0$ odd-photon destructive interference between the incident and generated fields is strongly inhibited for $\theta \neq 0$; second, most importantly, the cooperative frequency shift is strongly enhanced for small, but nonzero, values of θ due to the factor $(1 - \cos\theta)^{-1}$, which is not present if the generated radiation field is not considered self-consistently in the Maxwell-Bloch equations.

The remaining sections of the paper are organized as follows. In Sec. II, we describe the experimental setup and present the main FWM data. The theoretical treatment based on the Maxwell-Bloch equations is introduced in Sec. III, and in Sec. IV these equations are used to discuss the unveiled interesting features. Finally, closing remarks are presented in Sec. V.

II. EXPERIMENT

The experimental setup and the excitation scheme are displayed in Fig. 1. An Nd:YAG laser (pulse duration 10 ns and repetition rate 5 Hz) is frequency doubled and used to pump a dye laser with a wavelength of approximately 602 nm and a linewidth of 0.5 cm^{-1}. The dye laser with frequency ω_1 can be tuned to resonance via two-photon transitions from the ground state $5s$ to Rydberg levels $16d$ or $18s$. Part of the fundamental mode (IR) of the Nd:YAG laser, with fixed frequency ω_2 ($\lambda = 1.06\ \mu$m), is combined with the dye laser and the two beams, crossed at an angle θ, are focused into a sealed Rb cell. In the four-wave mixing process, a fourth photon is generated at frequency $\omega_3 = 2\omega_1 - \omega_2$ and brings the atoms back to the ground state. This fourth photon has a wavelength of approximately 420 nm, and it is close to the

*Present address: Joint Quantum Centre Durham-Newcastle, Department of Physics, Durham University, South Road, Durham DH1 3LE, United Kingdom.
†vianna@ufpe.br

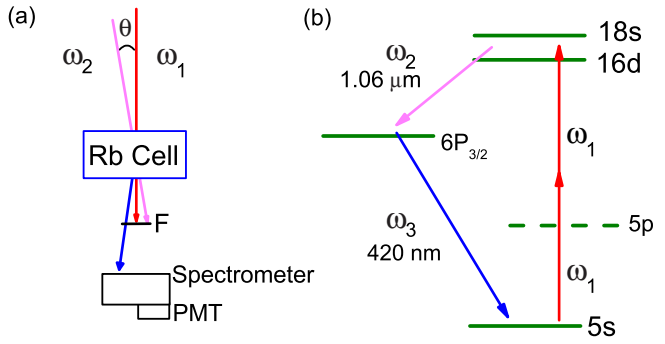

FIG. 1. (Color online) (a) Experimental setup, where the symbols PMT and F stand for the photomultiplier tube and filter, respectively. (b) Schematic representation of the energy levels of Rb that are relevant for the experiment, where ω_1 represents the dye laser frequency.

one-photon resonance with the transition $5s \rightarrow 6P_{3/2}$. The generated signal is analyzed in a monochromator and detected by a photomultiplier tube. The electronic processing of the signal is conducted using a boxcar and computer. The vapor cell, which is 5 cm long and contains both ^{85}Rb and ^{87}Rb isotopes in their natural abundances, with no buffer gas, can be heated to control the atomic density. Typically, we vary the atomic density from 10^{14} to 10^{16} atoms/cm^3.

Figure 2 shows the intensity of the FWM-generated signal as a function of the dye laser frequency detuning, $\Delta\omega = 2\omega_1 - \omega_{16d-5s}$, where $\omega_{16d-5s} \equiv (E_{16d} - E_{5s})/\hbar$, with E_{16d} being the energy of the state $16d$ and E_{5s} being the $5s$ ground-state energy. Each curve corresponds to the excitation spectrum for a specific crossing angle θ between the two incident beams. The results were obtained at atomic Rb density $N \approx 1 \times 10^{15}$ cm^{-3}, with the dye and IR beams having linear and parallel polarizations and intensities of 2 and 4 GW/cm^2, respectively. All curves were obtained for the same spectral range with the monochromator fixed at 420 nm and a window of order of 10 nm. Under this condition, we can observe two peaks associated with the two-photon resonant transitions, $5s$-$16d$ (at $\Delta\omega = 0$ cm^{-1}) and $5s$-$18s$ (at $\Delta\omega = 14.4$ cm^{-1}), and one peak at an intermediate frequency corresponding to the three-photon resonant transition $5s$-$6P_{3/2}$.

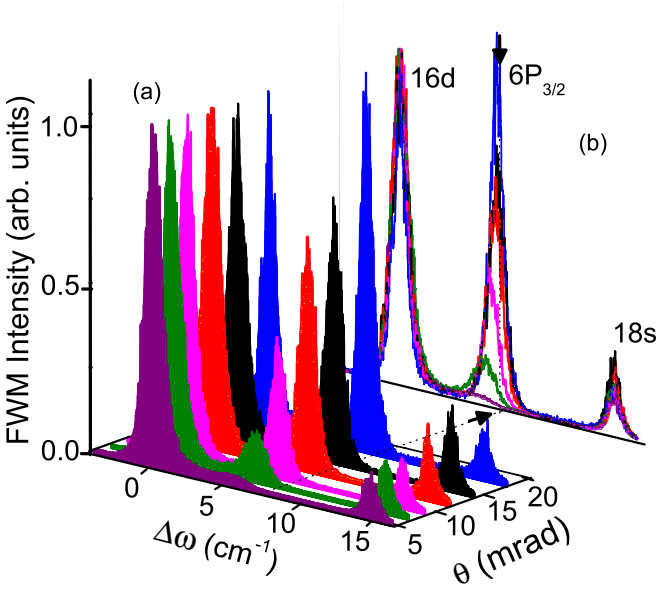

FIG. 2. (Color online) Four-wave mixing intensity as a function of the dye laser detuning $\Delta\omega$ relative to the two-photon transitions $5s \rightarrow 16d$ for different θ angles. Dye and IR beam intensities are $I_{\rm dye} = 2$ GW/cm^2 and $I_{\rm IR} = 4$ GW/cm^2. The atomic density is $N \approx 1 \times 10^{15}$ cm^{-3}. The curves are shown (a) horizontally displaced and (b) superposed (the dashed arrow indicates the position of the three-photon resonance).

In the collinear configuration, the focusing of the two beams in the middle of the cell allows for good phase matching, and a strong FWM signal is observed. However, as θ increases from 0 to 17 mrad, the phase mismatching also increases, causing a decrease in the intensity of the generated signal by two orders of magnitude. For comparison, the curves in Fig. 2(a) have the $16d$ peak intensity normalized to 1, and they are horizontally displaced. We also note that the intensity ratio between the $16d$ and $18s$ two-photon resonant peaks is almost constant, indicating that the signal generated at these two resonances presents a similar behavior in this range of θ. On the other hand, as θ increases, the $6P_{3/2}$ peak intensity, associated with the three-photon resonance, decreases more slowly when compared with the $16d$ peak intensity. In this case, the intensity variation behaves in such a way that the $16d$ and $6P_{3/2}$ peaks have almost the same intensity for $\theta \approx 17$ mrad.

Another salient feature is observed by superposing all curves, as shown in Fig. 2(b). First, we notice that the maximum intensity of the $16d$ and $18s$ peaks occurs always at the same dye laser excitation frequency. However, as θ decreases, the maximum intensity of the $6P_{3/2}$ peak exhibits a frequency shift to the red side, in comparison with the unperturbed three-photon resonance position (indicated by the arrow).

In Fig. 3, we compare the nonlinear response of the atomic system for two θ values as the atomic density increases:

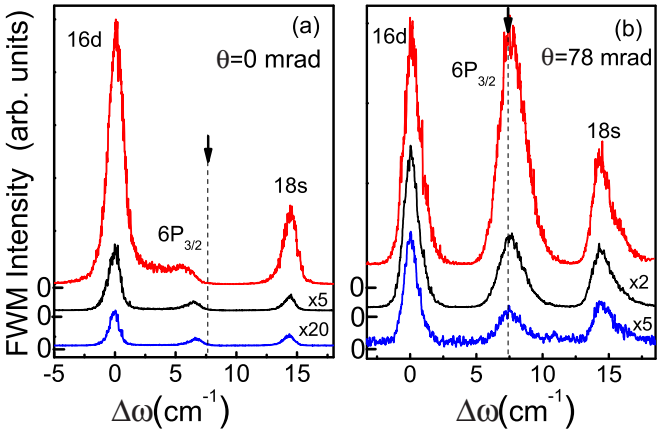

FIG. 3. (Color online) Four-wave mixing intensity as a function of the dye laser detuning $\Delta\omega$ relative to the two-photon transitions $5s \rightarrow 16d$ for different atomic densities. (a) $\theta = 0$ mrad and (b) $\theta = 78$ mrad (the arrows indicate the position of the three-photon resonance).

$\theta = 0$ mrad [Fig. 3(a)], collinear configuration, and $\theta =$ 78 mrad [Fig 3(b)]; from bottom to top, the curves correspond to $N \approx 0.5 \times 10^{15}$ cm^{-3}, $N \approx 1.0 \times 10^{15}$ cm^{-3}, and $N \approx 5.0 \times 10^{15}$ cm^{-3}, respectively. Again, for both values of θ, there is no variation on the dye laser excitation frequency for the $16d$ and $18s$ peaks, indicating no dependence on the atomic density; however, the $6P_{3/2}$ peak displays a θ-dependent behavior. In the collinear configuration [Fig. 3(a)], when all beams are propagating along the forward direction, including the generated blue beam, we observe an odd-photon destructive interference that becomes more important as the atomic density increases. As discussed in Ref. [16], the interaction of the atomic system with the new generated beam leads to a competition between two out-of-phase excitation pathways. Therefore, as the angle increases, the superposition between the incident and generated beams decreases, and the interference disappears as observed for $\theta = 78$ mrad. As mentioned before, at large values of θ the phase mismatching is quite large, and the signal is very small. Regardless, we can clearly see in Fig. 3(b) that the $6P_{3/2}$ peaks appear at the same excitation frequency, indicating no dependence on the atomic density, with the position of the peaks at the frequency of the three-photon resonance. We also verify that, as expected for a nonlinear signal, the intensity increases as N^2, indicating no odd-photon destructive interference.

III. THEORETICAL MODEL

The main features observed in Figs. 2 and 3 can be described by a model based on the density-matrix formalism applied to a four-level system. In particular, the scheme of levels shown in Fig. 1 allows the possibility of developing different processes in a complex and highly nonlinear manner. As discussed by Boyd [7], under two-photon resonant excitation conditions, competition between coherent (FWM) and incoherent (amplified spontaneous emission) nonlinear optical processes can occur.

For low-field intensities, we can solve Liouville's equation

$$\frac{\partial \hat{\rho}}{\partial t} = \frac{-i}{\hbar}[\hat{H}, \hat{\rho}] + (\text{relaxation terms}), \tag{1}$$

following the perturbative treatment given in Ref. [14]. We denote the levels $|5s\rangle$, $|6P_{3/2}\rangle$, $|16d\rangle$, and $|18s\rangle$ by $|a\rangle$, $|b\rangle$, $|d\rangle$, and $|s\rangle$, respectively, and the peaks by the quantum numbers nl associated with the involved resonances. The Hamiltonian of the system in the rotating frame is given by $\hat{H} = \hat{H}_0 + \hat{H}_{\text{int}}$, where $\hat{H}_0$ is the Hamiltonian of the free atom, and

$$\begin{aligned}\hat{H}_{\text{int}} = &-\hbar\Omega_{ad}^{(2)} e^{i2k_1 z}|a\rangle\langle d| - \hbar\Omega_{as}^{(2)} e^{i2k_1 z}|a\rangle\langle s| \\ &-\hbar\Omega_{bd} e^{ik_2 z}|b\rangle\langle d| - \hbar\Omega_{bs} e^{ik_2 z}|b\rangle\langle s| \\ &-\hbar\Omega_{ab} e^{ik_3 z}|a\rangle\langle b| + \text{H.c.}\end{aligned} \tag{2}$$

describes the electric-dipole coupling of the atom with the electromagnetic field

$$E(z,t) = \sum_{i=1}^{3} \frac{1}{2}[\mathcal{E}_i e^{-i\omega_i t + ik_i z} + \text{c.c.}], \tag{3}$$

where the fields with frequencies ω_1 and ω_2 are the incident ones and that with frequency ω_3 is the generated radiation field. Here $\Omega_{kl} = (1/2\hbar)\mu_{kl}\mathcal{E}_m$ is the Rabi frequency with the electric dipole matrix element μ_{kl}, $\mathcal{E}_m$ is the amplitude of the most resonant field with the $|k\rangle \longleftrightarrow |l\rangle$ transition, and $\Omega_{ia}^{(2)} = \sum_j \Omega_{ij}\Omega_{ja}/(\omega_{ja} - \omega_1)$ is the two-photon Rabi frequency with $i = d$ or s.

We are interested in the internally generated four-wave mixing field at frequency $\omega_3 = 2\omega_1 - \omega_2$, which is determined by the density-matrix element ρ_{ba}. As the atomic polarization is related to the density matrix through $P = N\langle\mu\rangle = Ntr(\rho\mu)$, ρ_{ba} must be solved in order to be consistent with Maxwell's equations.

The steady-state solution for $\sigma_{ba} = \rho_{ba}\exp(i\omega_3 t - ik_3 z)$ is calculated in the rotating-wave approximation and by applying perturbation theory up to second order in the dye laser field ($\mathcal{E}_1$) and up to first order in both the IR field ($\mathcal{E}_2$) and generated field ($\mathcal{E}_3$). The steady-state solution is supported by the rapid destruction of the induced coherence in the atomic system caused by the short coherence time of the nanosecond lasers. Under these conditions, σ_{ba} can be written as the sum of two terms:

$$\begin{aligned}\sigma_{ba} = &-\frac{\Omega_{ba}}{\Delta'_{ba} + i\gamma_{ab}} \\ &+ \left[\frac{\Omega_{da}^{(2)}\,\Omega_{bd}}{\Delta_{da} + i\gamma_{ad}} + \frac{\Omega_{sa}^{(2)}\,\Omega_{bs}}{\Delta_{sa} + i\gamma_{as}}\right]\frac{e^{-i\Delta k z}}{\Delta'_{ba} + i\gamma_{ab}},\end{aligned} \tag{4}$$

where we have introduced the detunings $\Delta_{ia} = 2\omega_1 - \omega_{ia}$ for $i = d$ or s and $\Delta'_{ba} = 2\omega_1 - \omega_2 - \omega_{ba}$ and also the relaxation rates γ_{ab} and γ_{ai},. The first term corresponds to the linear interaction of the atomic system with the internally generated field, while the second term describes the nonlinear interaction with the incident fields and takes into account the contributions of the two neighboring $16d$ and $18s$ Rydberg levels. Hyperfine structure and Doppler broadening, which are unresolved by the lasers, are neglected. In this equation, $\Delta k = (\vec{k}_3 - 2\vec{k}_1 + \vec{k}_2)_z$ is the component of the wave-vector mismatch in the generated field propagation direction, and it exhibits a dependency on the angle between the two incident fields θ given by

$$\Delta k = \frac{(2\omega_1 - \omega_2)}{c}\left[1 - \left(1 + \frac{8\omega_1\omega_2\left[\sin\left(\frac{\theta}{2}\right)\right]^2}{(2\omega_1 - \omega_2)^2}\right)^{\frac{1}{2}}\right]. \tag{5}$$

At high atomic densities, as in the present experiment, where the mean spacing between the atoms is of the order of $\langle r\rangle \sim \lambda/20$ ($Nk^{-3} \sim 100$), the light generated at $\omega_3 = 2\omega_1 - \omega_2 \equiv (E_{6p} - E_{5s})/\hbar$ is resonantly absorbed in a distance less than a wavelength. In this case, the polarization of the neighboring atoms gives rise to an effective field, called the local field or Lorentz field, $\mathcal{E}_3^L$ [17,18]. The relationship between the local field and the macroscopic field $\mathcal{E}_3$ that enters in Maxwell's equations is given by the Lorentz-Lorenz relation [19]: $\mathcal{E}_3^L = \mathcal{E}_3 - P_3/3\epsilon_0$, where P_3 is the polarization of the medium at frequency ω_3. This local field correction results in a shift in the resonance frequency known as the Lorentz shift Δ_{LL}, which, in the present study, modifies the three-photon resonance position Δ'_{ab} of Eq. (4) to $\Delta_{ba} = \Delta'_{ba} + \Delta_{LL}$, where $\Delta_{LL} = N\mu_{ab}^2/3\hbar\epsilon_0$ [5,18].

The four-wave-mixing field is calculated using Maxwell's equations in the slowly varying amplitude approximation. We

thus find

$$\frac{\partial \Omega_{ba}}{\partial z} = i\kappa_{ab}\sigma_{ba}, \tag{6}$$

where $\kappa_{ab} = N(k_3\mu_{ab}^2/2\hbar\epsilon_0)$ and σ_{ba} is given by Eq. (4). Therefore, Eq. (6) allows us to determine Ω_{ba}, i.e., the generated radiation field $\mathcal{E}_3$, in a self-consistent fashion through the emission and reabsorption of photons by the atoms in the sample.

Assuming now that at the entrance of the cell there is no radiation field at frequency ω_3, $\Omega_{ba}(z=0) = 0$, and neglecting depletion of the incident beams, we can obtain an analytical expression for the Rabi frequency of the generated beam at the end of the cell with a thickness z:

$$\Omega_{ba}(z) = i\kappa_{ab}F(\Delta_{ba})R(\Delta_{ia})\left[\frac{e^{-i\Delta kz} - e^{-i\kappa_{ab}F(\Delta_{ba})z}}{i\kappa_{ab}F(\Delta_{ba}) - i\Delta k}\right], \tag{7}$$

where the function

$$F(\Delta_{ba}) = \frac{1}{\Delta'_{ba} + \Delta_{LL} + i\gamma_{ab}}$$

contains the three-photon resonance with the Lorentz shift, while the function

$$R(\Delta_{ia}) = \left[\frac{\Omega_{da}^{(2)}\,\Omega_{bd}}{\Delta_{da} + i\gamma_{ad}} + \frac{\Omega_{sa}^{(2)}\,\Omega_{bs}}{\Delta_{sa} + i\gamma_{as}}\right]$$

describes the two-photon resonances with levels $16d$ and $18s$.

IV. ANALYSIS AND DISCUSSION

The theory developed in the previous section allows us to predict the shape and dependence of the FWM signal as a function of the dye laser frequency and its dependence on the crossing angle between the two incident beams. In order to do so, it is necessary to take into account the Clebsch-Gordan coefficients when calculating the effective couplings. We also need the relaxation rates, which are not purely radiative. Instead of estimating the ionization cross sections involved in the one- and two-photon processes, we prefer to use the parameters adjusted through the spectra obtained at low atomic density, as described in Ref [15]. For $N \approx 10^{14}$ cm^{-3}, we obtain $\gamma_{ai} \approx 0.1$ cm^{-1} for the two Rydberg levels and the value of $\gamma_{ab} \approx 0.5$ cm^{-1} for the $6P_{3/2}$ peak, which is limited by the linewidth of the IR beam. We also take into account the finite linewidth of the dye laser and perform a convolution of its measured Gaussian line shape.

A detailed discussion of the excitation spectrum of the FWM signal in the collinear configuration, when $\theta = 0$, is given in Ref. [15]. As shown, at high atomic density, a self-broadening contribution proportional to the atomic density needs to be consider for the two Rydberg levels. In this case, the total relaxation rates are given by $\Gamma_{nl} = \gamma_{nl} + \Gamma_{\rm self} = \gamma_{nl} + \beta N$, where the adjusted values for the self-broadening were $\beta/2\pi = (2.1 \pm 0.9) \times 10^{-12}$ MHz cm^3 and $\beta(16d)/\beta(18s) = \sqrt{3}$. It is interesting to note that this collinear configuration is described by Eq. (7) when $\Delta k = 0$ and can be written as

$$\Omega_{ba}(z) = R(\Delta_{ia})[1 - e^{-i\kappa_{ab}F(\Delta_{ba})z}]. \tag{8}$$

For the condition of $\theta = 0$, the exponential term of Eq. (8) goes to zero at high atomic density, yielding a limit form to Ω_{ba} that, used in Eq. (4), gives $\sigma_{ba} = 0$. This means that at elevated concentrations and on the three-photon resonance, $5s$-$6P_{3/2}$, the generated polarization becomes zero, characterizing the odd-photon destructive interference as described in Ref. [16].

For the noncollinear configuration the experimental results indicate a strong dependence on the crossing angle between the two incident beams. Focusing our attention on this noncollinear configuration, we consider $\theta \neq 0$ and rewrite Eq. (7) by combining the denominators related to the three-photon resonance:

$$\Omega_{ba}(z) = \frac{\left(\frac{\kappa_{ab}}{\Delta k}\right)}{\Delta_{ba} - \frac{\kappa_{ab}}{\Delta k} + i\gamma_{ab}} R(\Delta_{ia})[e^{-i\Delta kz} - e^{-i\kappa_{ab}F(\Delta_{ba})z}]. \tag{9}$$

Since $\theta \neq 0$, we are out of the condition of odd-photon destructive interference. Remarkably, we have now a term that explicitly exhibits the dependence on the crossing angle of the three-photon peak position when compared with the unperturbed resonance. This frequency shift term is given by

$$\Delta_{\rm coop} = -\frac{\kappa_{ab}}{\Delta k} \tag{10}$$

and appears only if we consider the interaction of the atomic system with the internally generated radiation field derived via Eqs. (6) and (7). The strong dependence on the crossing angle is given by the phase-matching coefficient [2,20,21]. Similar behavior was observed in xenon using three-photon excitation and multiphoton ionization techniques [22,23] and also through a third-harmonic generation process [24].

We note that both Δ_{LL} and $\Delta_{\rm coop}$ move the position of the three-photon peak to lower energy; that is, the peak shifts to a position closer to the $16d$ peak. However, the Lorentz shift does not depend on θ, and for a small crossing angle, such as those studied in the present experiment, $\Delta_{\rm coop}$ is much higher than Δ_{LL}. Therefore, we shall neglect the local field corrections and focus our attention on the θ dependence of the cooperative frequency shift.

The theoretical curves for the FWM excitation spectra at different angles can be obtained by numerical integration of Eq. (7), and the results are depicted in Fig. 4. To compare these results with the experimental data plotted in Fig. 2, the $16d$ peak intensity was also normalized to 1. The qualitative agreement between the experiment and theory with respect to the shape of the resonances, the intensity relations, and the shift of the three-photon peak to the red side is very rewarding.

A quantitative comparison of the intensity relation between the peaks as a function of the crossing angle θ between the incident beams is shown in Fig. 5. The symbols represent the experimental data, and the solid lines are from the theoretical calculation, corresponding to three values of dye laser frequencies in resonance with the $16d$, $18s$, and $6P_{3/2}$ levels. The calculations are performed neglecting the laser linewidths and using the maximum intensity of the $16d$ peak at the collinear configuration as a normalization parameter. In

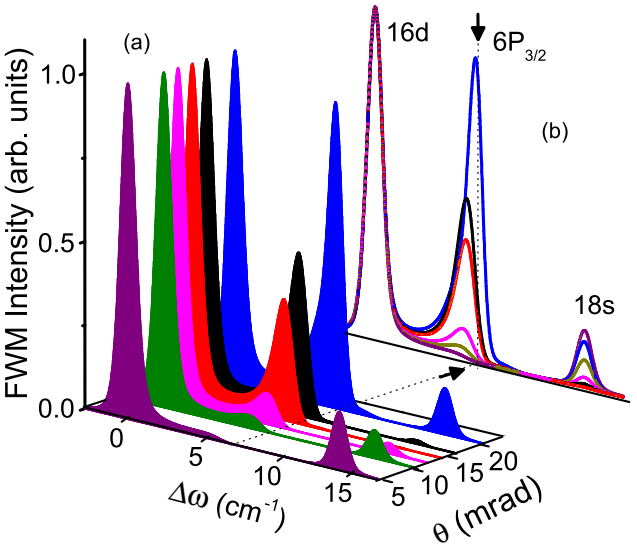

FIG. 4. (Color online) Theoretical calculation for the four-wave mixing intensity as a function of the dye laser detuning $\Delta\omega$ relative to the two-photon transitions $5s \rightarrow 16d$ for different θ angles [from Eq. (7)]. The atomic density is $N \approx 1 \times 10^{15}$ cm^{-3}. The curves are shown (a) horizontally displaced and (b) superposed (the arrow indicates the position of the three-photon resonance).

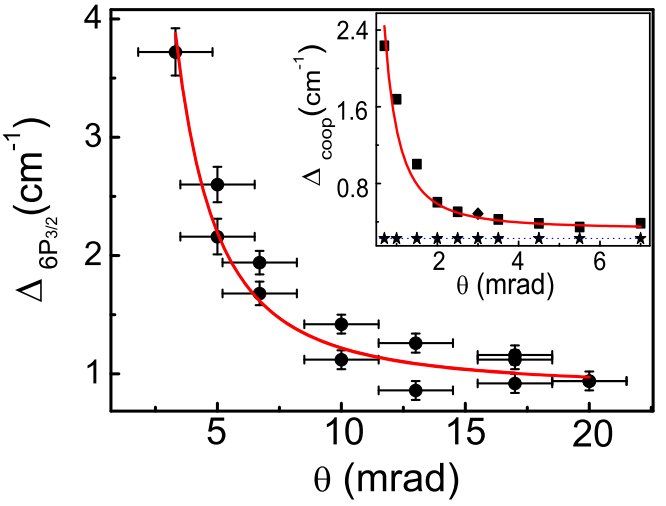

FIG. 6. (Color online) Frequency difference between the position of the three-photon resonance and the three-photon peak position as a function of θ for the experimental measurements (dots), $\Delta_{6P_{3/2}}$, and, in the inset, for the theoretical values (squares), Δ_{coop}. The stars in the inset are the results considering the phase-matching contribution but neglecting the interaction with the internally generated radiation field. The solid red lines are fits using Eq. (10).

this way, we obtain a good description not only of the intensity variation with θ but also of the intensity relation between the peaks. However, for $\theta \gtrsim 14$ mrad, the signal is very weak, and we do not have the resolution to observe the oscillatory behavior in the intensity of the generated beam, given by the square of Eq. (7), due to the propagation and phase-matching effects.

The frequency shift in the three-photon peak position can be measured from the experimental excitation spectra presented in Fig. 2 and compared with corresponding theoretical spectra shown in Fig. 4. The frequency difference between the position of the three-photon resonance and the three-photon peak position as a function of θ is shown in Fig. 6, where the dots are the experimental measure $\Delta_{6P_{3/2}}$ and the squares in the inset correspond to the theoretical values Δ_{coop}. Measurements of the frequency shift from the excitation spectra allow us to consider effects like the linewidth of the lasers and the self-broadening relaxation rates. However, we can use Eq. (10) to directly analyze the dependence on θ [21–23]. In the limit for small angles, the cooperative frequency shift can be written as

$$\Delta_{\text{coop}} = -\frac{\kappa_{ab}}{\Delta k} \approx \frac{c(2\omega_1 - \omega_2)\kappa_{ab}}{2\omega_1\omega_2[1 - \cos(\theta)]} = \frac{D}{1 - \cos(\theta)}, \quad (11)$$

where $\theta \neq 0$. The solid lines in Fig. 6 are fits of the experimental and theoretical results using Eq. (11). The adjusted coefficients are $D_{\text{exp}} = (1.5 \pm 0.8) \times 10^{-5}$ cm^{-1} for the experimental measurements and $D_{\text{theo}} = (5 \pm 1) \times 10^{-5}$ cm^{-1} for the calculate values. Despite the difference between theoretical and experimental values of D, it is clear that Eq. (11) describes the behavior of the red frequency shift with θ.

We have also plotted in the inset of Fig. 6 (stars) the frequency shift obtained by the theoretical calculation when we neglect the interaction of the atoms with the internally generated radiation field. Under this condition, we have solved Eq. (6) by considering only the contribution of the second term of σ_{ba} in Eq. (4). Although we have taken into account the phase-matching coefficient given by Eq. (5), for the parameters used in the present work, no θ dependence is obtained. This result reinforces our statement that the underlying mechanism responsible for the observed frequency shift comes from the quite strong cooperative effect between the atoms by the reabsorbing photons of the generated radiation field.

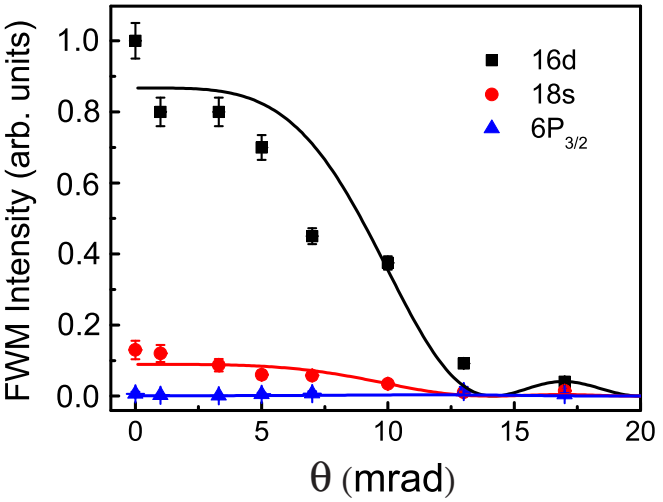

FIG. 5. (Color online) Peak intensity variation as a function of θ at the two-photon resonances, $16d$ and $18s$, and at the three-photon resonance.

V. CONCLUSIONS

We have investigated the nonlinear response of a rubidium vapor, in which two- and three-photon resonant transitions are driven by a four-wave-mixing process using two beams in a noncollinear configuration, i.e., $\theta \neq 0$, and high atomic density. In particular, the coherence induced on the three-photon resonant transition from $5s$ to $6p$ states, excited via intermediate Rydberg states, unveiled interesting features related to the interaction of the atoms with the internally generated radiation field. These features required a careful interpretation. First, the $\theta = 0$ (collinear configuration) odd-photon destructive interference between the incident and generated fields is strongly inhibited for $\theta \neq 0$. Second, most importantly, a cooperative frequency shift of the three-photon transition is not present if the generated radiation field is not considered self-consistently in the Maxwell-Bloch equations. Remarkably, this shift is strongly enhanced for small, but nonzero, values of θ due to the factor $(1 - \cos\theta)^{-1}$, in agreement with the description based on a cooperative frequency shift.

ACKNOWLEDGMENT

This work was supported by CNPq, FACEPE, and CAPES (Brazilian agencies).

[1] R. H. Dicke, Coherence in Spontaneous Radiation Processes, Phys. Rev. **93**, 99 (1954).

[2] R. Friedberg, S. R. Hartmann, and J. T. Manassah, Frequency shifts in emission and absorption by resonant systems of two-level atoms, Phys. Rep. C **7**, 101 (1973).

[3] M. O. Scully, E. S. Fry, C. H. R. Ooi, and K. Wódkiewicz, Directed Spontaneous Emission from an Extended Ensemble of N Atoms: Timing Is Everything, Phys. Rev. Lett. **96**, 010501 (2006); M. O. Scully, Collective Lamb Shift in Single Photon Dick Superradiance, *ibid.* **102**, 143601 (2009).

[4] R. Röhlsberger, K. Schlage, B. Sahoo, S. Couet, and R. Rüffer, Collective Lamb Shift in Single-Photon Superradiance, Science **328**, 1248 (2010).

[5] J. Keaveney, A. Sargsyan, U. Krohn, I. G. Hughes, D. Sarkisyan, and C. S. Adams, Cooperative Lamb Shift in an Atomic Vapor Layer of Nanometer Thickness, Phys. Rev. Lett. **108**, 173601 (2012).

[6] Z. Meir, O. Schwartz, E. Shahmoon, D. Oron, and R. Ozeri, Cooperative Lamb Shift in a Mesoscopic Atomic Array, Phys. Rev. Lett. **113**, 193002 (2014).

[7] R. W. Boyd, M. S. Malcuit, D. J. Gauthier, and K. Rzażewski, Competition between amplified spontaneous emission and the four-wave-mixing process, Phys. Rev. A **35**, 1648 (1987).

[8] H. Nagai and T. Nakanaga, Competition between two-photon-resonant three-photon ionization and four-wave mixing in Xe, Phys. Rev. A **84**, 063408 (2011).

[9] L. Deng, M. G. Payne, and W. R. Garrett, Effects of multi-photon interferences from internally generated fields in strongly resonant systems, Phys. Rep. **429**, 123 (2006), and references therein.

[10] A. Armyras, D. Pentaris, T. Efthimiopoulos, N. Merlemis, and A. Lyras, Saturation and population transfer of a two-photon excited four-level potassium atom, J. Phys. B **44**, 165401 (2011).

[11] R. T. Willis, F. E. Becerra, L. A. Orozco, and S. L. Rolston, Four-wave mixing in the diamond configuration in an atomic vapor, Phys. Rev. A **79**, 033814 (2009).

[12] A. Kölle, G. Epple, H. Kübler, W. R. Löw, and T. Pfau, Four-wave mixing involving Rydberg states in thermal vapor, Phys. Rev. A **85**, 063821 (2012).

[13] Y. O. Dudin and A. Kuzmich, Strongly Interacting Rydberg Excitations of a Cold Atomic Gas, Science **336**, 887 (2012).

[14] S. S. Vianna, P. Nussenzveig, W. C. Magno, and J. W. R. Tabosa, Polarization dependence and interference in four-wave mixing with Rydberg levels in rubidium vapor, Phys. Rev. A **58**, 3000 (1998).

[15] N. R. Melo and S. S. Vianna, Two-photon resonant forward four-wave mixing in rubidium vapor involving Rydberg states, J. Opt. Soc. Am. B **31**, 1735 (2014).

[16] M. G. Payne, L. Deng, and W. R. Garrett, Theory of the effect of odd-photon destructive interference on optical shifts in resonantly enhanced multiphoton excitation and ionization, Phys. Rev. A **58**, 1361 (1998).

[17] H. A. Lorentz, *The Theory of Electrons*, 2nd ed. (Dover, New York, 1952).

[18] J. J. Maki, M. S. Malcuit, J. E. Sipe, and R. W. Boyd, Linear and nonlinear optical measurements of the Lorentz local field, Phys. Rev. Lett. **67**, 972 (1991).

[19] J. D. Jackson, *Classical Electrodynamics*, 3rd ed. (Wiley, New York, 1998).

[20] R. Friedberg, S. R. Hartmann, and J. T. Manassah, Frequency shift in three-photon resonance, Phys. Rev. A **39**, 93 (1989).

[21] R. Friedberg, S. R. Hartmann, and J. T. Manassah, Three-photon frequency shift on non-collinear excitation, J. Phys. B **22**, 2211 (1989).

[22] W. R. Ferrell, M. G. Payne, and W. R. Garrett, Resonance broadening and shifting of spectral lines in xenon and krypton, Phys. Rev. A **36**, 81 (1987).

[23] W. R. Garrett, R. C. Hart, J. E. Wray, I. Datskou, and M. G. Payne, Large multiple collective line shifts observed in three-photon excitations of Xe, Phys. Rev. Lett. **64**, 1717 (1990).

[24] V. E. Peet and R. V. Tsubin, Gas-phase generation of resonance-enhanced third harmonic with crossed laser beams, Opt. Commun. **214**, 381 (2002).